Characterization of aerosol particles at Cape Verde close to sea and cloud level heights - Part 2: ice nucleating particles in air, cloud and seawater

Xianda Gong[1], Heike Wex[1], Manuela van Pinxteren[1], Nadja Triesch[1], Khanneh Wadinga Fomba[1], Jasmin Lubitz[1], Christian Stolle[2,3], Tiera-Brandy Robinson[3], Thomas Müller[1], Hartmut Herrmann[1], and Frank Stratmann[1]

[1]Leibniz Institute for Tropospheric Research, Leipzig, Germany
[2]Leibniz-Institute for Baltic Sea Research Warnemünde (IOW), Rostock, Germany
[3]Institute for Chemistry and Biology of the Marine Environment, University of Oldenburg, Wilhelmshaven, Germany

Correspondence: Xianda Gong (gong@tropos.de)

Abstract. Ice nucleating particles (INPs) in the troposphere can form ice in clouds via heterogeneous ice nucleation. Yet, atmospheric number concentrations of INPs (N_{INP}) are not well characterized and although there is some understanding of their sources, it is still unclear to what extend different sources contribute, nor if all sources are known. In this work, we examined properties of INPs at Cape Verde from different sources, the oceanic sea surface microlayer (SML) and underlying
5 water (ULW), the atmosphere close to both sea and cloud level as well as cloud water.

Both enrichment and depletion of N_{INP} in SML compared to ULW were observed. The enrichment factor (EF) varied from roughly 0.4 to 11, and there was no clear trend in EF with temperature.

N_{INP} in PM_{10} sampled at Cape Verde Atmospheric Observatory (CVAO) at any particular temperature spanned around 1 order of magnitude below -15 °C, and about 2 orders of magnitude at warmer temperatures (>-12 °C). N_{INP} in PM_1 were
10 generally lower than those in PM_{10} at CVAO. About $83\pm22\%$, $67\pm18\%$ and $77\pm14\%$ (median±standard deviation) of INPs had a diameter >1 μm at ice activation temperatures of -12, -15, and -18 °C, respectively. Among the 17 PM_{10} samples at CVAO, three PM_{10} filters showed elevated N_{INP} at warm temperatures, e.g., above 0.01 std L^{-1} at -10 °C. However, for N_{INP} in PM_1 at CVAO, this is not the case. At these higher temperatures, often biological particles have been found to be ice active. Consequently, the difference in N_{INP} between PM_1 and PM_{10} at CVAO, suggests that biological ice active particles
15 were present in the super-micron size range.

N_{INP} in PM_{10} at CVAO was found to be similar to that on Monte Verde (MV, at 744 m a.s.l) during non-cloud events. During cloud events, most INPs on MV were activated to cloud droplets. When highly ice active particles were present in PM_{10} filters at CVAO, they were not observed in PM_{10} filters on MV, but in cloud water samples, instead. This is direct evidence that these INPs which are likely biological are activated to cloud droplets during cloud events.

20 In general, Cape Verde was often affected by dust from the Saharan desert during our measurement. For the observed air masses, atmospheric N_{INP} in air fit well to the concentrations observed in cloud water. When comparing concentrations of both sea salt and INPs in both seawater and PM_{10} filters, it can be concluded that sea spray aerosol (SSA) only contributed a minor

fraction to the atmospheric N_{INP}. Therefore it can be said that, unless there would be a significant enrichment of N_{INP} during the formation of SSA particles, N_{INP} was mainly dominated by mineral dust at cold temperatures with few contributions from possible biological particles at warmer temperatures.

1 Introduction

5 Ice particle formation in tropospheric clouds can affect cloud properties such as cloud lifetime, their radiative effects on the atmosphere, and the formation of precipitation (Hoose and Möhler, 2012; Murray et al., 2012). Ice crystals in the atmosphere can be formed either via homogeneous nucleation below $-38\,^{\circ}$C or heterogeneous nucleation aided by aerosol particles known as ice nucleating particles (INPs) at warmer temperatures ($>-38\,^{\circ}$C). Immersion freezing refers to the process when an INP becomes immersed in an aqueous solution e.g., through the process of cloud droplet activation (Vali et al., 2015). Immersion
10 freezing is suggested to be the most important freezing process for mixed phase clouds (Ansmann et al., 2008; Westbrook and Illingworth, 2013), and is the process we will focus on in this study.

Dust particles are recognized as effective INPs below $-20\,^{\circ}$C (Augustin-Bauditz et al., 2014) or even below $-15\,^{\circ}$C (Hoose and Möhler, 2012; Murray et al., 2012). Laboratory studies on natural mineral dusts from different regions have been conducted to quantify the particle's ability to nucleate ice (Niemand et al., 2012; DeMott et al., 2015). Mineral dust particles from deserts
15 are composed of a variety of minerals, and K-feldspar is supposed to be more effective for ice nucleation than other minerals in the mixed-phase cloud temperature regime (Atkinson et al., 2013; Augustin-Bauditz et al., 2014; Niedermeier et al., 2015). However, overall, desert dust particles from diverse sources show comparable ice nucleating efficiency (Boose et al., 2016). Different parameterizations have been employed to summarize the mineral dust particle's ice nucleating ability (Niemand et al., 2012; Ullrich et al., 2017).

20 A few field measurements have been carried out to quantify the ice nucleation properties of desert dust. Based on airborne measurements, DeMott et al. (2003) found that ice nucleating aerosol particles in air masses over Florida had sources from the North African dust. Chou et al. (2011) observed a good correlation between the number concentration of larger particles and INP number concentration (N_{INP}) during a Saharan dust event at the Jungfraujoch in the Swiss Alps. Collecting airborne dust over the Saharan desert, Price et al. (2018) observed two orders of magnitude variability in N_{INP} at any particular temperature
25 from ~ -13 to $\sim -25\,^{\circ}$C, which was related to the variability in atmospheric dust loading, while desert dust's ice-nucleating activity was only weakly dependent on the differences in desert sources. Schrod et al. (2017) found that mineral dust or a constituent related to dust was a major contributor to the ice nucleating properties of the aerosol on Cyprus, and N_{INP} in elevated dust plumes was on average a factor of 10 higher than at ground level.

Ocean water can be a potential source of INPs (Brier and Kline, 1959) which would originate from the biosphere. The
30 source of INPs in ocean water might be associated with phytoplankton blooms (Schnell and Vali, 1976). Recently, Wilson et al. (2015) and Irish et al. (2017) found that organic material, with a diameter $<0.2\,\mu$m, is the major ice nucleator in the sea surface microlayer (SML). Based on a long-term measurement of INPs in the marine boundary layer in the south of and around Australia, Bigg (1973) suggested that INPs in ambient air were contributed by marine aerosol particles. DeMott et al. (2016)

found that INPs from laboratory generated sea spray aerosol (SSA) aligned well with measurements from diverse regions over the oceans. Further evidence of a connection between marine biological activity and N_{INP} was uncovered in their laboratory study (DeMott et al., 2016). In pristine marine conditions, such as the Southern Ocean, SSA was the main source of the INP population, but N_{INP} was relatively low in the Southern Ocean as well as in the clean marine Northeast Atlantic (McCluskey

5 et al., 2018a, b). These field measurements are consistent with the model work by Burrows et al. (2013), which emphasizes the importance of SSA contribution to INPs in remote marine regions.

It is currently still uncertain whether the coarse mode particles or smaller particles are the major source of atmospheric INPs. Vali (1966) found that the diameters of INPs were mostly between 0.1 and 1 μm. On the high alpine research station Jungfraujoch, Mertes et al. (2007) found that ice residuals were as small as 300 nm and they were mostly present in the

10 submicron particle size range. Modeling studies also suggest that INP are a temperature dependent fraction of all particles with sizes above 500 nm (DeMott et al., 2010, 2015). Conen et al. (2017) found INPs at -8 °C were equally distributed amongst the particles with sizes up to 2.5 μm and with sizes between 2.5 and 10 μm. Other field measurements reported that coarse mode particles were more efficient INP, e.g., INPs (mainly bacterial aggregates and fungal spores) occurred in the size range of 2 - 6 μm (Huffman et al., 2013). Mason et al. (2016) found for Arctic aerosol that 91±9%, 79±17%, and 63±21% of INPs

15 had an aerodynamic diameter of >1 μm at ice activation temperatures of -15, -20, and -25 °C, respectively. Creamean et al. (2018) also found that super-micron or coarse mode particles are the most proficient INPs at warmer temperatures in the Arctic and they might be biological INPs. Concerning biological INP, it should be mentioned that it is well understood by now that these feature macromolecules of only some ten nanometers in size at the most (Pummer et al., 2015). Some of them are easily separated from their carrier (e.g., from pollen and fungal spores), while others are embedded in the cell membrane (e.g., for

20 bacteria), but based on these above cited literature results, it seems that most of the biological INPs still occur together with their original carrier in the atmosphere.

Direct measurement of N_{INP} in the cloud water can be used to estimate concentrations of INPs in the air. Joly et al. (2014) measured total and biological (i.e., heat-sensitive) INPs between -5 to -14 °C in samples from the summit of Puy de Dôme (1465 m a.s.l., France). Petters and Wright (2015) summarized many INP spectra obtained from rain water, melted sleet, snow

25 and hail samples at different sampling locations and reported a range of N_{INP} for these precipitation samples. Based on a shipborne measurement of the east coast of Nova Scotia, Canada, Schnell (1977) directly compared N_{INP} in the seawater to that in the fog water and found that N_{INP} in fog water and seawater appeared to vary quite independently of each other. As one part of the here presented study, these field measurement values will be compared with values obtained from our measurement campaign in the framework of the MarParCloud (Marine biological production, organic aerosol particles and marine clouds: a

30 Process Chain) project.

During the MarParCloud project, samples collected for INPs analysis include: SML and underlying water (ULW) from the ocean upwind of the island; quartz fiber filter samples of atmospheric aerosol, collected on a tower installed at the island shore (inlet height: 42 m a.s.l) and on a mountaintop (inlet height: 746 m a.s.l); and cloud water collected during cloud events on the mountaintop. In this study, we will first discuss N_{INP} in the SML and ULW. We will then discuss N_{INP} in the air,

35 including a comparison of N_{INP} in PM_{10} and PM_1 and a comparison of N_{INP} close to both sea and cloud level. Lastly, N_{INP}

in the cloud water will be discussed. In addition, we will provide a feasible way to link N_{INP} in ambient air, ocean water and cloud water. This connection can be drawn only during times when there were cloud events on the mountaintop, together with data on number concentrations on cloud condensation nuclei (N_{CCN}). Respective information was derived and discussed in an accompanying paper (Gong et al., 2019b). For more information about the campaign itself, we refer to an upcoming overview paper by van Pinxteren et al.

2 Experiment and methods

2.1 Sampling sites and sample types

2.1.1 Sampling site

The measurements were carried out on São Vicente island at Cape Verde from 13 September to 13 October, 2017. We set up three measurement stations at Cape Verde, at the Cape Verde Atmospheric Observatory (CVAO), on Monte Verde (MV) and an Ocean Station (OS). CVAO (16°51′49 N, 24°52′02 W) is located in the northwestern shore of the island of São Vicente, 70 m from the coastline about 10 m a.s.l. Filter samplers were installed on top of a 32 m tower. MV (16°52′11 N, 24°56′02 W) is located on a mountaintop (744 m a.s.l), ∼7 km away to the west of CVAO. Filter samplers were situated on the ground, upwind of any installations on the mountaintop. The OS covered an area at ∼16°53′30 N, ∼24°54′00 W, with a distance of at least 5 km from the island. Details on the measurement site and the meteorological conditions can be found in the accompanying paper (Gong et al., 2019b). In short, the conditions at Cape Verde were quite stable, with temperature of on average 26.6 °C at CVAO and 21.2 °C at MV and wind speeds between 0.6 and 9.7 m s^{-1} with directions from the northeast.

In the following, the different samples collected during the campaign are described in detail. All of these samples were stored at −20 °C right after sampling. After the campaign the long-term storage and transport of the collected samples from Cape Verde to the Leibniz Institute for Tropospheric Research (TROPOS), Germany was carried out in a cooled container at −20 °C. At TROPOS, all samples were again stored frozen at −20 °C until analysis was done. Measurement sites, locations, sample types and additional information are summarized in Tab. 1.

Following the description of the sampling, we will briefly introduce the measurement methods related to INPs, including freezing devices, N_{INP} calculation and measurement uncertainties. Note that all the times presented here are in UTC (corresponding to local time +1). For better comparison, all ambient particle number concentrations in this study are given for standard temperature and pressure (STP, 0 °C and 1013.25 hPa).

2.1.2 Seawater sampling

Seawater samples were taken at the OS by using a fishing boat at a distance of at least 5 km from the coast (off-shore samples). The SML samples were collected using a glass plate sampler (Harvey and Burzell, 1972; Irish et al., 2017; van Pinxteren et al., 2017). The glass plate had a surface area of 2000 cm^{-2} and was immersed vertically into the ocean and then withdrawn at a slow rate (between 5 to 10 cm s^{-1}) and allowed to drain for less than 5 s. The surface film adhering to the surface of the

Table 1. Measurement sites, locations, sample types and measurement instruments.

Measurement site	Location	Sample type	Instrument
CVAO	16°51′49 N, 24°52′02 W	PM_1 quartz fiber filter	INDA
	inlet height: 42 m a.s.l	PM_{10} quartz fiber filter	INDA
MV	16°52′11 N, 24°56′02 W	PM_{10} quartz fiber filter	INDA
	inlet height: 746 m a.s.l	Cloud water	LINA, INDA
OS	∼16°53′30 N, ∼24°54′00 W	SML	LINA, INDA
		ULW	LINA, INDA

glass was scraped off from both sides of the glass plate with a framed Teflon wiper into a 1 liter glass bottle. For each SML sample, several liters were collected and 1 liter was required ∼55 dips. Based on the amount of material collected, the number of dips and the area of the plate, the averaged thickness of the layer collected was calculated as ∼91.0 μm. ULW samples were collected at the same time and location as the SML samples. ULW was collected from a depth of 1 m by a specially

5   designed device, which consists of a glass bottle mounted on a telescopic rod in order to monitor sampling depth. The bottle was opened underwater at the intended sampling depth with a specifically designed seal-opener. After collection, the glass bottles containing both the SML and ULW samples were kept in a freezer at −20 °C up to the analysis. During the campaign, 9 SML and 9 ULW samples were collected for INP analysis. Details of SML and ULW samples, including the sampling time, location, salinity and additional information are provided in the supplement, Tab. S1.

10   **2.1.3   Aerosol particle sampling**

Particle sampling was done using high-volume samplers with either a PM_{10}-inlet and or a PM_1-inlet (Digitel filter sampler DHA-80, Walter Riemer Messtechnik, Germany) operating with an average flow rate of ∼500 L min^{-1} for 24 hours sampling periods. The high-volume samples were collected on 150 mm quartz fiber (Munktell, MK 360) filters. The filters were preheated in our laboratory at 110 °C for 24 hours to remove the organic carbon background. After sampling, the filters were transported

15   to a freezer where they were kept at −20 °C. For INP analysis, a fraction of these filters of 2 cm^2 was used. From CVAO, there were 17 and 19 filters from PM_{10} and PM_1 collection (CVAO PM_{10} and CVAO PM_1), respectively, and at MV, 17 filters were collected for PM_{10} (MV PM_{10}). Field blind filters were obtained by inserting clean filters into the Digitel sampler for a period of 24 hours without loading them. Three blind filters were collected during this campaign. Details of filter samples, including sampling time, duration, total volume and additional information can be found in the supplement, Tab. S2 (CVAO

20   PM_{10}), Tab. S3 (CVAO PM_1) and Tab. S4 (MV PM_{10}).

2.1.4 Cloud water sampling

During the campaign, MV was in clouds roughly 58% of the time (a detailed analysis on this can be found in Gong et al. (2019b)). Cloud water was collected with CASCC2 (Caltech Active Strand Cloud Collector Version 2) at MV. All cloud drop sizes were collected in one bulk sample. Drops were collected by inertial impaction on Teflon strands with a diameter of 508

5 μm. The 50% lower size cut for the CASCC2 was approximately 3.5 μm diameter. The flow rate through the CASCC2 was approximately 5.8 m^3 min^{-1}. The CASCC2 is described in more details in Demoz et al. (1996). Between cloud events, the cloud water sampler was cleaned with a large amount ($\sim$5 L) of ultrapure water. Once the collector was cleaned, a blank was taken by spraying about 200 mL of ultrapure water into the collection strands in the collector and subsequent sampling of this water. After collection, the cloud water samples were kept in a freezer at $-20\,^{\circ}$C. During the campaign, 13 cloud samples were

10 collected for INP analysis. The details of cloud samples, including sampling time, duration, volume and additional information are provided in the supplement, Tab. S5.

2.2 Freezing devices

Two droplet freezing devices called LINA (Leipzig Ice Nucleation Array) and INDA (Ice Nucleation Droplet Array) have been set up at TROPOS in Germany. The design of LINA was inspired by Budke and Koop (2015). Briefly, 90 droplets with the

15 volume of 1 μL were pipetted from the samples onto a thin hydrophobic glass slide, with each droplet being placed separately into its own compartment. After pipetting, the compartments were sealed at the top with another glass slide, to prevent the droplets from evaporation and to prevent ice seeding from neighboring droplets. The droplets were cooled on a Peltier element with a cooling rate of 1 K min^{-1} down to $-35\,^{\circ}$C, while the setup was illuminated by a circular light source from above. Once the cooling started, pictures were taken every 6 s by a camera. The number of frozen versus unfrozen droplets was derived

20 automatically by an image identification program in Python. LINA was employed to measure SML, ULW and cloud water samples in this study. More detailed parameters and the temperature calibration of LINA and its application can be found in previous studies (Chen et al., 2018; Gong et al., 2019a).

The design of INDA was inspired by Conen et al. (2012), but deploying PCR-trays instead of separate tubes. For quartz fiber filters, circular pieces with a diameter of 1 mm were punched out. Each of the 96 wells of a PCR-tray were filled with

25 the filter piece together with 50 μL of ultrapure water. For SML, ULW and cloud water samples, 50 μL of the water samples was filled into each PCR-tray. After sealing by a transparent foil, the PCR-tray was placed on a sample holder and immersed into a bath thermostat, where it was illuminated from below with a LED light source. The bath thermostat then decreased the temperature with a cooling rate of approximately 1 K min^{-1}. Real-time images of the PCR-tray were recorded every 6 s by a CCD (charge-coupled device) camera. Frozen droplets can be identified based on the brightness change during the freezing

30 process. A program recorded the actual temperature of the cooling bath and related it to the real-time images from the CCD camera. The temperature in the PCR-trays had been calibrated. More detailed parameters and temperature calibration of INDA and its application can be found in previous studies (Chen et al., 2018; Hartmann et al., 2019).

2.3 Deriving N_{INP}

2.3.1 Basic calculation

Based on Vali (1971), the cumulative concentration of INP (N_{INP}) as a function of temperature per air or water volume can be calculated by:

$$N_{\text{INP}}(\theta) = \frac{-\ln(1 - f_{\text{ice}}(\theta))}{V} \tag{1}$$

with

$$f_{\text{ice}}(\theta) = \frac{N(\theta)}{N_{\text{total}}} \tag{2}$$

where N_{total} is the number of droplets and $N(\theta)$ is the number of frozen droplets at temperature θ. Eq. 1 accounts for the possibility of the presence of multiple INPs in one vial by assuming that INPs are Poisson distributed. As for the quartz fiber filters, V is the volume of air collected onto one circular 1 mm filter piece placed in each well, resulting in airborne N_{INP}. The information of the air volume can be found in the supplement, Tab. S2, Tab. S3 and Tab. S4. As for the SML, ULW and cloud water, V is the volume of droplet/well (V_{LINA}=1 μL, V_{INDA}=50 μL), resulting in N_{INP} per volume of water. Compared to the droplets examined in a LINA measurement, INDA measurements have a larger volume of water in each well. The larger volume of water corresponds to a higher probability of the presence of INPs in each well, therefore INDA can detect INPs at warmer temperatures, where INP are more scarce. In this study, the derived N_{INP} from LINA and INDA measurements were combined when both instruments were deployed.

2.3.2 Uncertainty and background

Because the number of INPs present in the washing water is usually small (some single up to a few tens of INPs per examined droplet/well), and the number of droplets/wells considered in our measurements is limited, statistical errors need to be considered in the data evaluation. Therefore, confidence intervals for f_{ice} were determined using the method suggested by Agresti and Coull (1998). Previous studies (McCluskey et al., 2018a; Suski et al., 2018; Gong et al., 2019a) used the same method to calculate the freezing devices' measurement uncertainties.

For the quartz fiber filters, a background freezing signal resulting from the field blind filters was determined by doing a regular INDA measurement with these filters. Measured N_{INP} from the sampled filters was corrected by subtracting the averaged background concentrations determined for the blind filters. A detailed explanation of background subtraction can be found in the supplement of Wex et al. (2019). All values for airborne N_{INP} presented in the following are background-corrected.

2.3.3 Salinity correction of SML and ULW

SML and ULW samples were adjusted to account for the freezing depression caused by dissolved salts in sea water. First, based on Kreidenweis et al. (2005), the water activity can be calculated by:

$$a_{\text{w}} = \frac{n_{\text{water}}}{n_{\text{water}} + i * n_{\text{solute}}} \tag{3}$$

where the n_{solute} and n_{water} are the number of moles of solute and water in solution, respectively. i is the van't Hoff factor (Pruppacher and Klett, 2010). We assumed sea salt to be mainly sodium chloride, for which the van't Hoff factor is 2. The freezing depression temperature as a function of a_{w} was taken from Koop and Zobrist (2009). In our study, this was roughly a correction by 2.2 °C.

5 **2.4 Active surface site density**

A thorough analysis of particle number size distributions (PNSDs) has been presented in Gong et al. (2019b), and based on these PNSDs we derived the particle surface area size distributions (PASDs) for use in this study (to be seen in the supplement, Fig. S10). This provides an opportunity to determine the temperature-dependent cumulative active surface site density (n_{s}) for aerosol particles. The n_{s} is a measure of how well an aerosol acts as a seed surface for ice nucleation. The n_{s} can be calculated

10 as:

$$n_{\text{s}} = \frac{N_{\text{INP}}(\theta)}{A_{\text{total}}} \tag{4}$$

Where A_{total} is the concentration of the total particle surface area.

3 Results

3.1 INP in SML and ULW

15 Based on Eq. 1, the derived N_{INP} in seawater as a function of temperature is shown in Fig. 1, for both SML and ULW. Error bars show the 95% confidence interval. For completeness, f_{ice} of all seawater samples is shown in the supplement, Fig. S1 (measured by LINA) and Fig. S2 (measured by INDA). The variation of N_{INP} at any particular temperature is within one order of magnitude. Included in Fig. 1 are previous studies of N_{INP} measured east of Greenland in the Arctic (shown as red box) and east of America in the North Atlantic Ocean (shown as black box) from Wilson et al. (2015).

20 The concentration range detected for ULW in Wilson et al. (2015) (both in the Arctic and the North Atlantic Ocean) roughly agrees with our data. In Wilson et al. (2015), N_{INP} in the SML in the North Atlantic Ocean is at the lower end of that found in the Arctic. A possible reason for this difference could be the biological activity of the ocean water. Wilson et al. (2015) found that organic material was correlated to N_{INP} in SML, and that N_{INP} per gram of total organic carbon in the Arctic and the North Atlantic Ocean were comparable. A recent study found that the SML at Cape Verde was oligotrophic, which is supported by the

25 low Chlorophyll a and transparent exopolymer particles concentrations found during the MarParCloud campaign (Robinson et al., 2019). This could be the reason why N_{INP} in SML in this study is lower than those reported in Wilson et al. (2015).

To better quantify the enrichment or depletion of N_{INP} in SML to ULW, we derived an enrichment factor (EF). The EF in SML was calculated by dividing N_{INP} in SML ($N_{\text{INP, SML}}$) by the respective N_{INP} measured in ULW ($N_{\text{INP, ULW}}$), as the below equation shows:

30 $$\text{EF} = \frac{N_{\text{INP, SML}}}{N_{\text{INP, ULW}}} \tag{5}$$
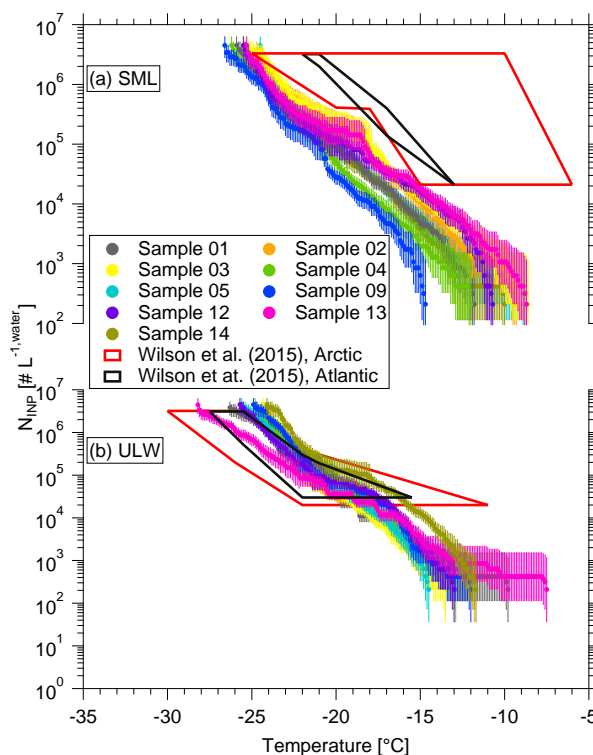
Figure 1. N_{INP} as a function of temperature in SML (a) and ULW (b). Error bars show the 95% confidence interval. Previous field measurements of N_{INP} in seawater by Wilson et al. (2015) are compared, as shown by red and black boxes.

Enrichment of N_{INP} in the SML is indicated when EF > 1, while depletion is indicated when EF < 1. Fig. 2 shows the EF as a function of temperature. Both enrichment and depletion were observed, but there is no clear trend of the EF with temperature. EF varied from 0.36 to 11.40 at $-15\,^\circ$C and from 0.36 to 7.11 at $-20\,^\circ$C. By comparing T_{10} (the temperature at which 10% of droplets had frozen) for the SML and ULW, Wilson et al. (2015) observed higher enrichment of INPs in SML in both the Arctic and the North Atlantic Ocean. However, Irish et al. (2017) observed both enrichment and depletion of INPs in SML in the Arctic, similar to the observation made in the present study.

These differences in EF between studies might partially due to differences in the techniques deployed in our and the other studies. SML samples were about $\sim$91.0 µm thick in this study, while for Wilson et al. (2015) those were between 6 to 83 µm.

3.2 N_{INP} in air

Three different sets of filter samples were collected at CVAO and MV, i.e., CVAO PM$_{10}$, CVAO PM$_1$ and MV PM$_{10}$. In the this section, we will discuss N_{INP} at CVAO for the two different size classes and compare N_{INP} from close to the sea level (CVAO) to that at cloud level (MV).
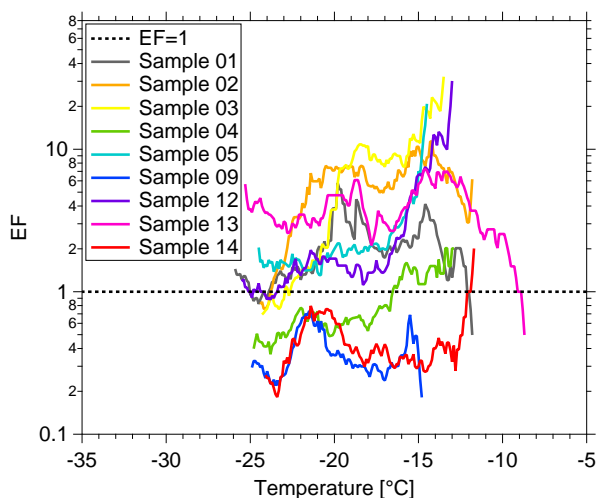
Figure 2. EF as function of temperature. The EF=1 is shown by dashed line.

3.2.1 N_{INP} close to sea level

CVAO PM$_{10}$

N_{INP} as a function of temperature from CVAO PM$_{10}$ filters and CVAO PM$_1$ filters are shown in Fig. 3(a) and (b). Error bars show the 95% confidence interval. The respective vales of f_{ice} are shown in the supplement, Fig. S3 (CVAO PM$_{10}$) and Fig. S4

5   (CVAO PM$_1$), together with the results from the blind filters. The CVAO PM$_{10}$ filter samples were all active at $-11.3\,°$C and the highest freezing temperature was found to be $-5.0\,°$C. Filter samples collected in Cape Verde over the period 2009-2013 for INP measurement were reported by Welti et al. (2018), and they are shown as gray background in Fig. 3(a). The measured N_{INP} in this study is within the N_{INP} range presented by Welti et al. (2018).

N_{INP} at any particular temperature span around 1 order of magnitude below $-15\,°$C, and about 2 orders of magnitude

10   at warmer temperatures. This is consistent with the previous studies from O'Sullivan et al. (2018) and Gong et al. (2019a), who carried out field measurement in northwestern Europe and the eastern Mediterranean, respectively. A few samples (CVAO 1596, CVAO 1641 and CVAO 1643) showed elevated concentrations above $0.01\,\mathrm{std\,L^{-1}}$ at $-10\,°$C. Biological particles usually contribute to INPs at this moderate supercooling temperature (Kanji et al., 2017; O'Sullivan et al., 2018).

The correlation of N_{INP} at two different temperatures was calculated. For temperature steps of $0.1\,°$C, N_{INP} at every temper-

15   ature was correlated to that at every other temperature in the measurement range. With increasing difference in temperatures, the variation in N_{INP} at two temperatures become less correlated. As long as the examined temperature difference was less than $2\,°$C, N_{INP} were correlated. But when looking at this in a broader picture, in the temperature region down to $\sim -16.8\,°$C, N_{INP} at all temperatures correlated well with that at all other temperatures, with coefficient of determination (R^2) > 0.8 and p $<$ 0.01. The same was true for N_{INP} in the temperatures region $< -18.4\,°$C. In between these two temperature regimes (between

$>-16.8\ ^\circ$C and $<-18.4\ ^\circ$C), the correlation of N_{INP} was clearly lower. Therefore, it might be expected that INPs that are active in these two temperature regimes originated from different sources.
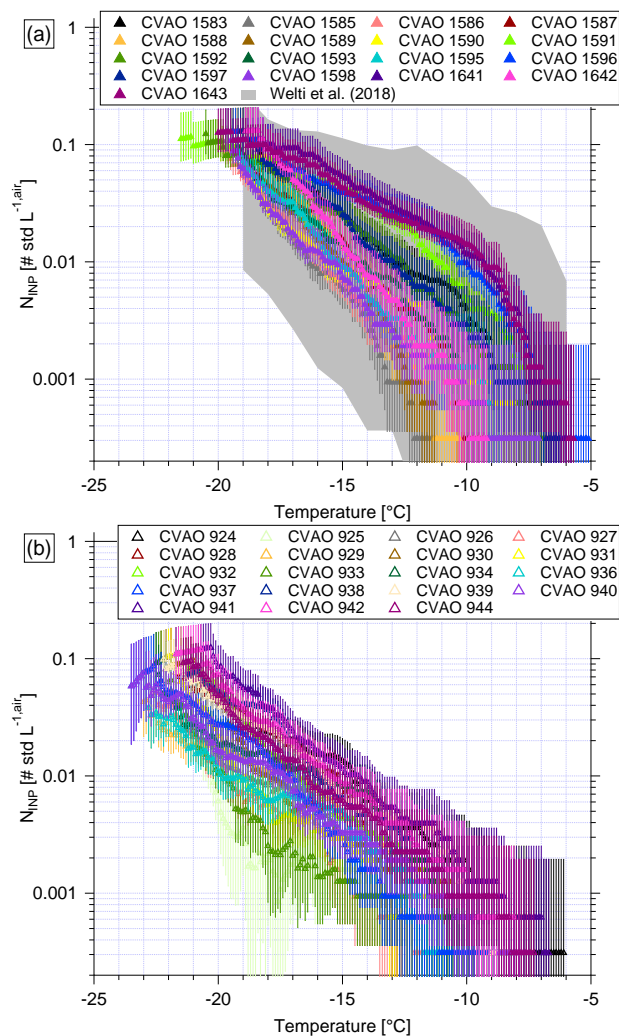
Figure 3. N_{INP} as a function of temperature from CVAO PM$_{10}$ filters (a) and CVAO PM$_1$ filters (b). The field measurement of N_{INP} in PM$_{10}$ by Welti et al. (2018) is shown by gray shadow in Fig. (a). Error bars show the 95% confidence interval.

CVAO PM$_1$ in comparison to CVAO PM$_{10}$

N_{INP} in PM$_1$ filters are also determined in this study (as shown in Fig. 3(b)). An initial observation of the data shows that the

5   bulk of the data of N_{INP} for CVAO PM$_1$ is below that for CVAO PM$_{10}$. Fig. 4 shows the probability density function (PDF) of N_{INP} in CVAO PM$_{10}$ (black) and CVAO PM$_1$ (red) at $-12\ ^\circ$C (a), $-15\ ^\circ$C (b) and $-18\ ^\circ$C (c). These temperatures were chosen because for each of them the filters contributes data. Comparing N_{INP} for PM$_1$ and PM$_{10}$, a few key features are evident:

1. Larger particles, i.e., super-micron ones, were more efficient INPs, which is independent of temperature in the examined range.

2. Smaller particles, i.e., submicron ones, exhibited an equal spread of about 1 order of magnitude in N_{INP} for the whole temperature range (see Fig. 3(b)). The elevated N_{INP} at warm temperatures which are seen for CVAO PM$_{10}$ are not observed for CVAO PM$_1$.
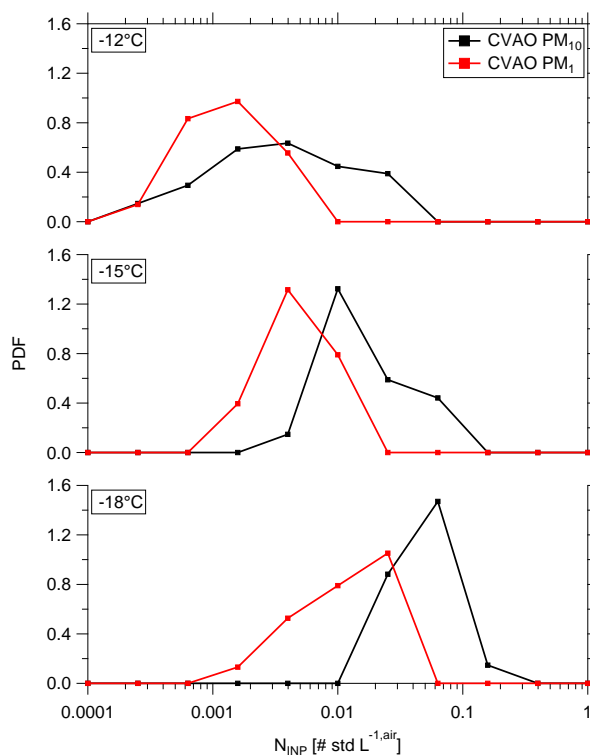
Figure 4. PDFs of N_{INP} measured from CVAO PM$_{10}$ filters by black line and CVAO PM$_1$ by red line at $-12°$C in the upper panel, $-15\,°$C in the middle panel and $-18°$C in the lower panel.

As for the first feature, we found that $83\pm22\%$, $67\pm18\%$ and $77\pm14\%$ (median$\pm$standard deviation) of INPs had a diameter of $>1\,\mu$m at ice activation temperatures of -12, -15, and $-18\,°$C, respectively. On average, over all temperatures, this INP number fraction for super-micron particles is roughly 70% (shown for a higher temperature resolution in Fig. 5), almost independent of temperature. Mason et al. (2016) and Creamean et al. (2018) also found that the majority of INPs is in the super-micron size range. However, they see even increasing fractions towards higher temperatures. For the present study, as said above, only three of the examined 17 filters showed clearly elevated N_{INP} at high temperatures, so overall such an increase was not observed.

As for the second feature, looking at Fig. 3(b), we found that N_{INP} spread about 1 order of magnitude at any temperature from -12 to $-20\,°$C. As outlined above, a few PM$_{10}$ samples showed elevated concentrations at warm temperatures, showing
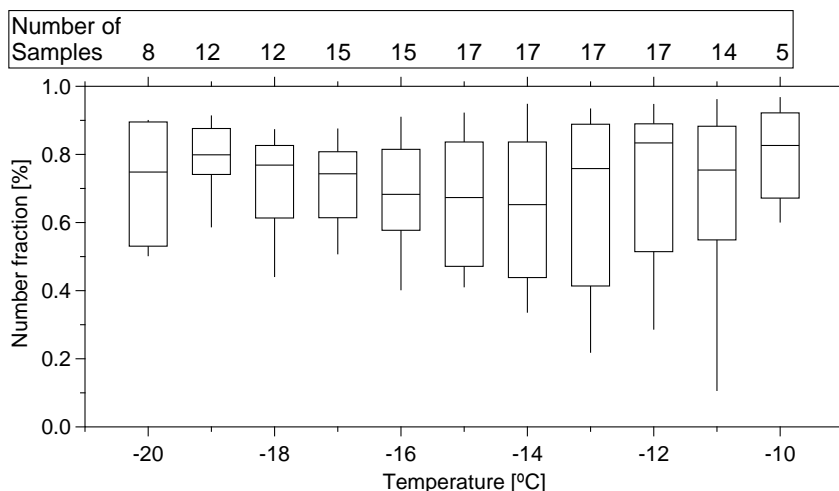
Figure 5. Boxplot of number fraction of INPs in the size range of >1 μm as a function of temperature. The number of samples indicated on top of the figure shows how many different samples contributed at the different temperatures.

up as a "bump" in the freezing curves at higher temperatures. This bump at warm temperatures was not observed for the CVAO PM$_1$ filters. N_{INP} of CVAO 932, CVAO 942 and CVAO 944 (sampled at the same time as CVAO 1596, CVAO 1641 and CVAO 1643) are all below 0.001 std L^{-1} at $-10°$C. As mentioned above, INP active at comparably high temperatures are generally assumed to be biological in origin (e.g., Kanji et al., 2017; O'Sullivan et al., 2018), and our findings suggest that there are

5   biological INPs in the CVAO PM$_{10}$ samples that are absent in the CVAO PM$_1$ samples, i.e., that these likely biological INPs are super-micron in size.

3.2.2 N_{INP} at cloud level

In the companion paper (Gong et al., 2019b), we discussed PNSD and CCN number concentration (N_{CCN}) at CVAO and MV. We found that particles are mainly well mixed in the marine boundary layer and derived the periods with cloud events, with

10   a time resolution of $\sim$30 minutes, at MV. In the present study, N_{INP} in PM$_{10}$ at CVAO and MV are compared. The fraction of time during which there was a cloud event to the total sampling time (cloud time fraction) for each filter is summarized in the supplement, Tab. S4. All of the filters were more or less affected by cloud events, with two filters being affected only little (cloud time fraction <10%), i.e., MV 1602 and MV 1603. When comparing results from these two filters to those from filters sampled at the same time at CVAO (see Fig. 6(a)), we found that N_{INP} are quite similar close to sea level (CVAO) and cloud

15   level (MV). This is in line with what was discussed in the companion paper (Gong et al., 2019b), i.e., the marine boundary is often well mixed at Cape Verde.

Fig. 6(b) compares N_{INP} at CVAO and MV when MV filters were mostly collected during cloud events with cloud time fractions >90%. During the cloud events, the filters did not collect droplets larger than 10 μm because of the inlet cutoff. It is obvious that for these cases, N_{INP} at MV is much lower than that at CVAO, implying that particularly INPs that were ice
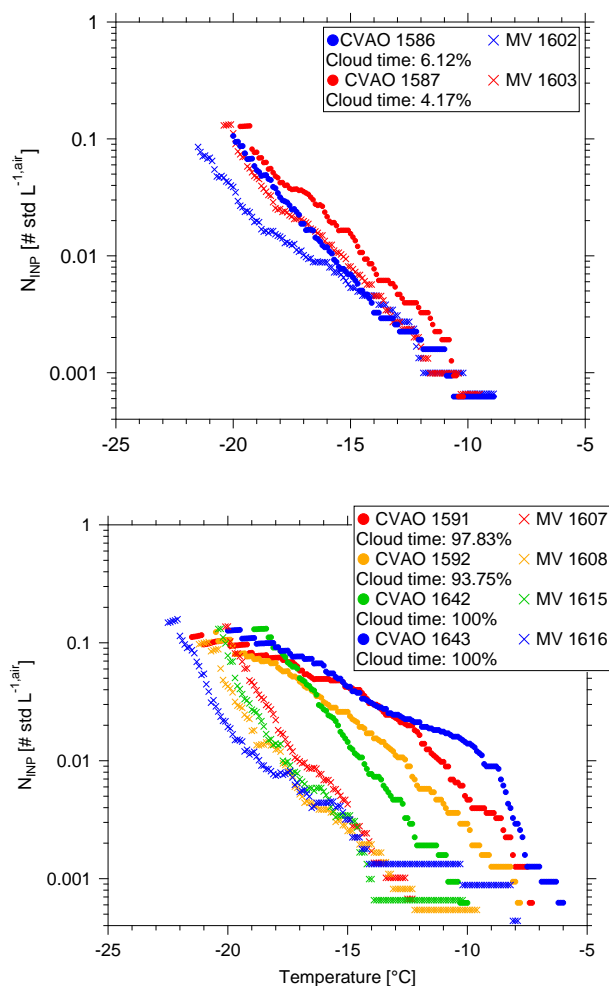
Figure 6. N_{INP} as a function of temperature from CVAO PM_{10} filters and MV PM_{10} filters during less (cloud time fraction <10%) cloud effected periods (a) and highly (cloud time fraction >90%) cloud effected periods (b).

active above $\sim -17\,°$ C were activated to cloud droplets to a large degree. But note that even when filters have a cloud time fraction of 100% (MV 1615 and MV 1616), the respective filters still had clearly more INPs on them than the field blind filters (see supplement, Fig S5). This might indicate that either not all INPs are activated to cloud droplets, or, on the other hand, that some INPs were only recently activated to a cloud droplet and the droplet size was smaller than 10 μm.

5   Concerning the super-micron particles of likely biological origin that activated ice already at $-10\,°$ C and above (Fig. 4), it is observed that the related corresponding bump is not seen in the corresponding data from MV (MV 1610, MV 1614 and MV 1616 - to be seen in the supplement, Fig. S6). This indicates that these INPs were all activated to cloud droplets during the cloud events, and we will come back to this below.

3.3 INP in cloud water

3.3.1 Main characteristics and N_{INP} in cloud water

Thirteen cloud water samples were collected during cloud events in this study. Sampling durations varied from 2.5 to 13 hours and volumes varied from 78 to 544 mL. The most abundant inorganic species were Na^+ and Cl^-, followed by SO_4^{2-}, NO_3^-

5 and Mg^{2+}. For example, the mass concentration of Na^+ and Cl^- varied from 5.00 to 46.11 and 9.27 to 70.30 mg L^{-1}, with a mean value of 17.31 and 28.86 mg L^{-1}, respectively. Gioda et al. (2009) found in Puerto Rico the Na^+ and Cl^- concentration in the cloud water varied from 3.79 to 15.53 and 5.90 to 23.20 mg L^{-1}, with a mean of 10.74 and 15.67 mg L^{-1}, respectively, which are comparable to this study. All of the above mentioned parameters are summarized in the supplement, Tab. S5.
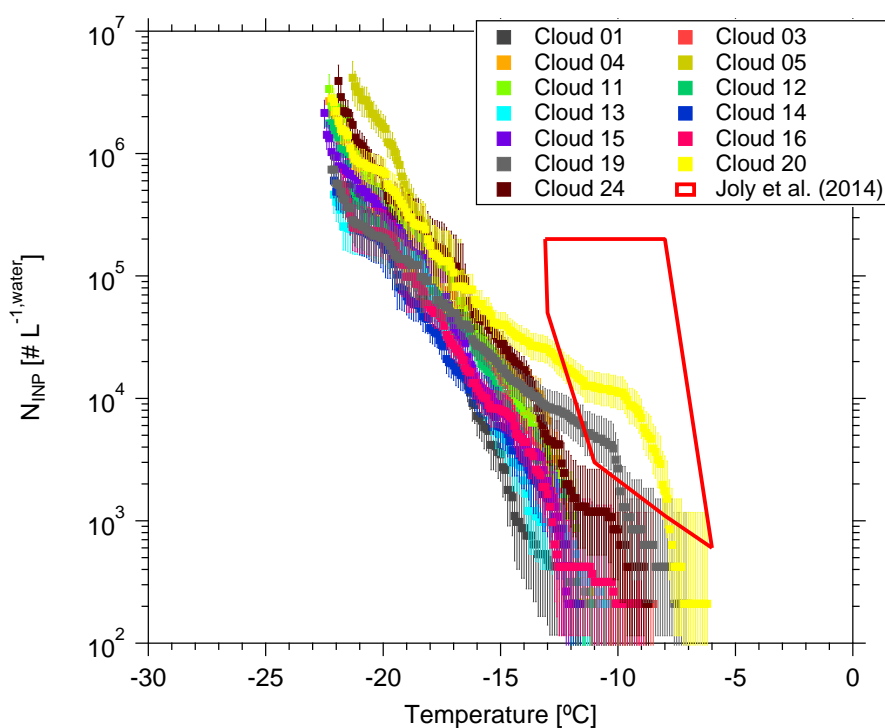
Figure 7. N_{INP} as a function of temperature in cloud water. Error bars show the 95% confidence interval. Previous field measurements of N_{INP} in cloud water by Joly et al. (2014) are compared, as shown by the red box.

Based on Eq. 1, the derived N_{INP} as a function of temperature is shown in Fig. 7. Error bars represent the 95% confidence

10 interval. For completeness, f_{ice} for cloud water is shown in the supplement, Fig. S8 (measured by LINA) and Fig. S9 (measured by INDA). N_{INP} at any particular temperature span less than 1 order of magnitude below $-15\,^{\circ}$C, while they span 2 orders of magnitude at warmer temperatures. We observed elevated N_{INP} in the cloud water at warm temperatures (above 1000 L^{-1} at $-10\,^{\circ}$C) particularly for the Cloud 19, Cloud 20 and Cloud 24 samples. Joly et al. (2014) measured the total and biological (i.e., heat-sensitive) INPs between -5 to -14°C from the summit of Puy de Dôme (1465 m a.s.l., France), as shown in the red

box in Fig. 7. Joly et al. (2014) observed very high concentrations of both biological particles and N_{INP}. Agreement of N_{INP} in cloud water all over the world was not expected, since the sources of INPs are different in different locations.

When highly ice active particles were present for CVAO PM$_{10}$ filters (CVAO 1596, CVAO 1641 and CVAO 1643), they were not observed for MV PM$_{10}$ (MV 1610, MV1614 and MV 1616, which had cloud time fractions of 52, 87 and 100%,

5 respectively), but instead were found in cloud water samples (Cloud 19, Cloud 20 and Cloud 24). This is in line with what was outlined in section 3.2.2 that these highly ice active particles were activated to cloud droplets during cloud events. Periods during which clouds were present at MV, together with the sampling periods of all cloud water samples and selected CVAO PM$_{10}$ filters (those that had higher N_{INP} at warm temperatures, CVAO 1596, CVAO 1641 and CVAO 1643) can be checked in the supplement, Fig. S7.

10 **3.3.2 Connecting INPs in the cloud water with these in the air**

In the following, N_{INP} in the cloud water will be compared to that in the air. To be able to do this, we used measured values of N_{CCN} to calculate cloud droplet number concentrations. These, together with an assumption on cloud droplet size (d_{drop}) yields the volume of cloud water per volume of air, given as $F_{\text{cloud\_air}}$ in Eq. 6:

$$F_{\text{cloud\_air}} = N_{\text{CCN}} * \pi/6 * d_{\text{drop}}^3 \tag{6}$$

15 For the calculation, we used N_{CCN} measured at CVAO at a supersaturation of 0.30% (Gong et al., 2019b). N_{CCN} was averaged for the different periods when each cloud water sample was collected. The chosen supersaturation corresponds to a critical diameter of roughly 80 nm, which is at the Hoppel minimum of the respective particle number size distributions (Gong et al., 2019b), indicating that this is indeed the relevant supersaturation occurring in the prevailing clouds. Based on previous studies (Miles et al., 2000; Bréon et al., 2002; Igel and Heever, 2017), we assumed that d_{drop} varies between 7 and 20 μm and

20 did separate estimates for these two values and additionally for 15 μm.

Following this approach, $F_{\text{cloud\_air}}$ varied from $4.2*10^{-7}$ to $1.1*10^{-6}$, with a median of $8.5*10^{-7}$. Previous studies used the liquid water content (LWC), which is a measure of the mass of the water in a cloud in a specified amount of dry air. Typical ranges for LWC in thicker clouds are between 0.2 and 0.8 g m^3 (Rangno and Hobbs, 2005; Petters and Wright, 2015), corresponding to $F_{\text{cloud\_air}}$ between $2*10^{-7}$ to $8*10^{-7}$, which agreed well with this study.

25 With this $F_{\text{cloud\_air}}$, N_{INP} in the respective volume of air can be compared to N_{INP} in this volume of cloud water when assuming that all INPs are CCN, which, based on the super-micron size of most of the INPs alone, is likely. To do so, N_{INP} obtained for cloud water was multiplied by $F_{\text{cloud\_air}}$ (for the three different assumptions on d_{drop}) to yield N_{INP} in the air ($N_{\text{INP,air}}$).

Fig. 8 shows the measured N_{INP} in the air as a function of temperature by squares. Derived $N_{\text{INP,air}}$ from cloud water

30 (calculated with a d_{drop} of 15μm) are shown by triangles. The samples with comparatively high numbers of INPs active at warm temperatures, are shown in different colors. CVAO 1596, CVAO 1641 and CVAO 1643 are shown by green squares (the rest shown by blue squares) and derived $N_{\text{INP,air}}$ from samples collected for Cloud 19, Cloud 20 and Cloud 24 are shown by

brown triangles (the rest shown by red triangles). The range of values indicated for $N_{INP,air}$ was obtained from using 7 and 20 μm cloud droplet size, with 7 μm droplets yielding the lower boundary and 20 μm the upper one.

There is general agreement between measured and derived N_{INP} in air, however, with some variation where the values derived from cloud water samples are somewhat lower. This might be connected to a less than optimal sampling efficiency of
5   the cloud water sampler, which has a 50% collection efficiency at 3.5 μm. Also the spread in the derived values, originating from the different assumed d_{drop}, is rather large. Nevertheless, it is striking that at least within an order of magnitude, based on our comparably simple assumptions, an agreement between concentrations of INP in the air and in cloud water is found.
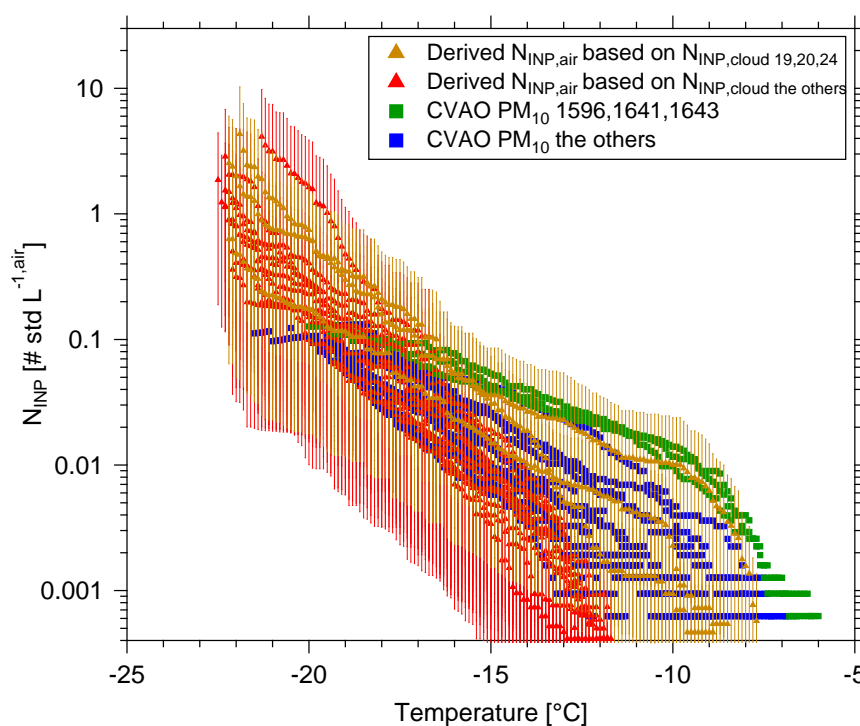
Figure 8. The measured N_{INP} as a function of temperature in the air by squares. The derived $N_{INP,air}$ based on INP concentrations measured for cloud water are shown by triangles. The samples with highly ice active INPs at warm temperatures, are shown in a different color than the others: CVAO 1596, CVAO 1641 and CVAO 1643 are shown by green squares and derived $N_{INP,air}$ based on Cloud 19, Cloud 20 and Cloud 24 are shown by brown triangles. The uncertainty range indicated for the derived $N_{INP,air}$ originate from calculations with 7 and 20 μm cloud droplet size.

3.4   INPs originating from sea spray

In the following section, it will briefly be discussed whether SSA contributed noticeably to INPs in the air. Assuming sea
10   salt and INPs to be similarly distributed in both, seawater and air (i.e., assuming that INPs would not be enriched during the

production of sea spray), N_{INP} in the air originating from sea spray ($N_{INP}^{sea\,spray,air}$) can be calculated based on Eq. 7:

$$N_{INP}^{sea\,spray,air} = \frac{NaCl_{mass,air}}{NaCl_{mass,seawater}} * N_{INP}^{seawater} \tag{7}$$

where $NaCl_{mass,air}$ and $NaCl_{mass,seawater}$ are sodium chloride mass concentrations in air and seawater, respectively. $N_{INP}^{seawater}$ is the INP number concentration in the seawater (this calculation can be done similarly for both SML and ULW).
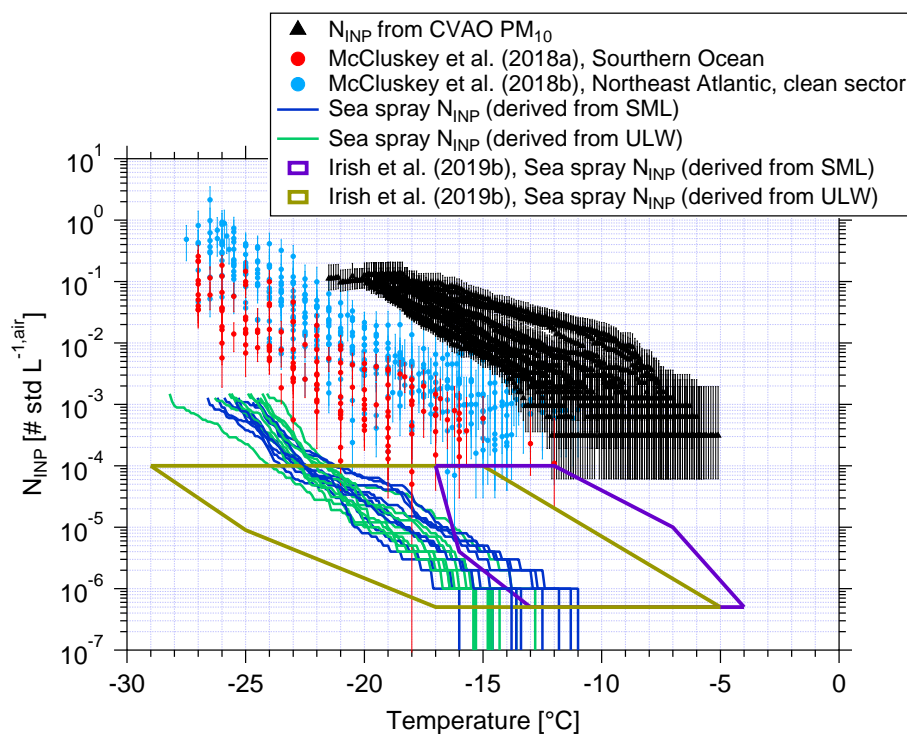
Figure 9. N_{INP} as a function of temperature from PM$_{10}$ filters (black triangles), and error bars show the 95% confidence interval. N_{INP} as a function of temperature from McCluskey et al. (2018a, b) are shown by red and light blue dots, respectively. Error bars show the 95% confidence interval. $N_{INP}^{sea\,spray,air}$ from this study are shown by blue (derived from SML) and green lines (derived from ULW). $N_{INP}^{sea\,spray,air}$ from Irish et al. (2019b) are shown by purple (derived from SML) and brown (derived from ULW) boxes.

5    $NaCl_{mass,air}$ and $NaCl_{mass,seawater}$ can be found in the supplement, Tab. S1 and Tab. S2. $NaCl_{mass,seawater}$ was very stable, with a median value ∼31 g L^{-1}. $NaCl_{mass,air}$ showed large variability from 3.40 to 17.76 mg L^{-1}, with a median of 13.08 mg L^{-1}. Based on Eq. 7, the resulting $N_{INP}^{sea\,spray,air}$ are shown in blue (derived from SML) and green (derived from ULW) in Fig. 9. Irish et al. (2019b) used the same method to get $N_{INP}^{sea\,spray,air}$ in the Arctic (without considering enrichment of INPs in sea salt particles during sea spray generation), as shown by purple (derived from SML) and brown (derived from ULW) boxes in

10   Fig. 9. As discussed in section 3.1, N_{INP} from ULW at Cape Verde are comparable to the Arctic, therefore, $N_{INP}^{sea\,spray,air}$ (derived from ULW) are also comparable. A high enrichment of N_{INP} in SML to ULW was observed in the Arctic (Irish et al., 2019b). Therefore, $N_{INP}^{sea\,spray,air}$ (derived from SML) in the Arctic was also higher than in this study.

Fig. 9 includes N_{INP} from PM_{10} in this study (shown by black triangles). These values are roughly 4 orders of magnitude above our $N_{\mathrm{INP}}^{\mathrm{sea\,spray,air}}$. But Fig. 9 also shows airborne N_{INP} as derived for the Southern Ocean (McCluskey et al., 2018a) and the Northeast Atlantic (only clean sector, McCluskey et al., 2018b), which are all above our $N_{\mathrm{INP}}^{\mathrm{sea\,spray,air}}$. As mentioned above, we did not consider a possible enrichment of INPs in SSA compared to the SML or ULW samples. Previous studies

5   found an enrichment of organic carbon in submicron sea spray particles of about 10^4 to 10^5 (Keene et al., 2007; van Pinxteren et al., 2017), and this value decreased to 10^2 for super-micron particles (Keene et al., 2007; Quinn et al., 2015). It is not clear if INPs are included in the organic carbon for which the enrichment was observed. Also, the INPs we detected in this study were mostly in the super-micron size range. If we increased $N_{\mathrm{INP}}^{\mathrm{sea\,spray,air}}$ by about 2 orders of magnitude in agreement to the enrichment observed for super-micron organic carbon, the resulting $N_{\mathrm{INP}}^{\mathrm{sea\,spray,air}}$ becomes comparable to sea spray INPs

10 measured in the Southern Ocean (McCluskey et al., 2018a) and the Northeast Atlantic (McCluskey et al., 2018b). But even when considering such an enrichment of INPs, INPs originating from sea spray would only explain a small fraction of all INPs contributing to the measured airborne N_{INP} in the air at Cape Verde.

4   Discussion

N_{INP} close to sea and cloud level height were compared. One major point of interest is to know whether ground-based mea-

15 surements can be used to infer aerosol properties at the cloud level. In this study, we found that N_{INP} are quite similar close to sea level (CVAO) and cloud level (MV) during non-cloud events. But it should still be noted that we only have a small number of filter samples representing non-cloud events in this study. During the observed cloud events, most INPs at MV are activated to cloud droplets. The above findings are in line with what was discussed in the companion paper (Gong et al., 2019b), i.e., (1) the marine boundary is often well mixed at Cape Verde and PNSDs and N_{CCN} are similar close to both sea and cloud level; (2)

20 during cloud events, larger particles are activated to cloud droplets.

Most INPs are in the super-micron size range at Cape Verde. We found that about 70% of INPs had a diameter of >1 μm at ice activation temperatures between -10 and $-20\,^{\circ}$C. Mason et al. (2016) and Creamean et al. (2018) also found that the majority of INPs is in the super-micron size range in the Arctic, in agreement with the results we obtained here.

Above we derived that N_{INP} contributed from SSA only accounted for a minor fraction of total N_{INP} in the air, as well as in

25 the cloud water at Cape Verde. This still holds even when considering a possible enrichment of INPs in SSA up to 10^2, which is an enrichment as given in literature for super-micron organic particles (Keene et al., 2007; Quinn et al., 2015). It can similarly be seen when considering that it has been described in literature that mineral dust is associated with a factor of 1000 higher ice surface site density (a measure to describe the ice activity per particle surface area), compared to SSA at temperatures from -12 to $-35\,^{\circ}$C (Niemand et al., 2012; DeMott et al., 2016; McCluskey et al., 2018a). In our study, the super-micron particles

30 that make up a large fraction of the INPs we observed were mainly mineral dust, as described in the accompanying study (Gong et al., 2019b). The comparably high ice activity of mineral dust and the presence of mainly dust particles in the super-micron size range in our study again supports that indeed most INPs observed in this study were not from sea spray. This is in line

with results from Si et al. (2018) and Irish et al. (2019a), both done in the Arctic, where it was also concluded that SSA only contributed little to the INP population.

While the above arguments suggest that INPs in our study were mostly mineral dust particles, there were also some measurements with comparably high INP concentrations at temperatures of $-10\,°C$ and above. It is an open question where these highly

5 ice active INPs originated. Such high ice activity is typically associated with biological particles. The times during which these highly ice active INPs were observed were times when air masses came from Southern Europe, travelling along the African coast and meanwhile crossing over the region of the Canary Islands. Therefore, for these specific samples, a contribution of INPs from these land sources might be assumed.
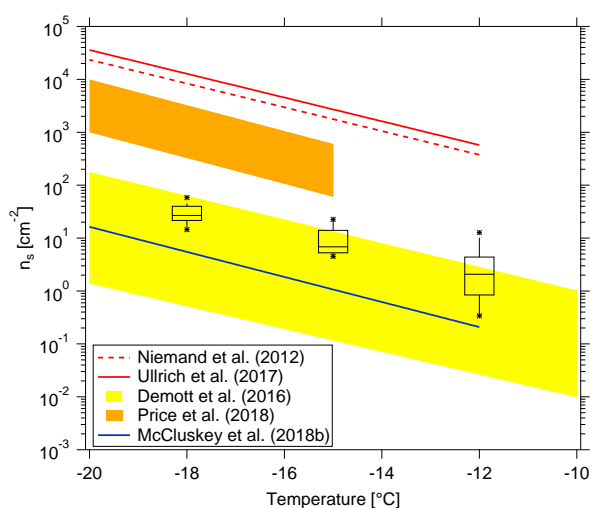
Figure 10. n_s as a function of temperature in this study is shown by black boxes. The boxes represent the interquartile range. Whiskers represent 10th to 90th percentile. Data not included between the whiskers are plotted as an outlier with a star. Two n_s parameterizations (Niemand et al., 2012; Ullrich et al., 2017) for pure desert dust are shown in dashed and solid red lines, respectively. n_s parameterizations from McCluskey et al. (2018b) for pristine SSA over the Northeast Atlantic are shown as a solid blue line. We also compare to recent data from airborne measurement in a dust layer by Price et al. (2018) in brown shadow and from nascent laboratory generated and ambient SSA by DeMott et al. (2016) in yellow shadow, respectively.

Finally, in Fig. 10, we show the surface site density derived for our data following Niemand et al. (2012) (details on the

10 surface area are given in the supplement, Fig. S10), together with parameterizations for n_s given by Niemand et al. (2012), Ullrich et al. (2017) and McCluskey et al. (2018b), and the measured n_s given by DeMott et al. (2016) and Price et al. (2018). Niemand et al. (2012) derived n_s from a laboratory study, based on aerosol consisting purely of desert dust particles. It is therefore reasonable that these mineral dust related n_s values are the largest values shown in Fig. 10, as they are purely related to the mineral dust surface area of an aerosol. All other values shown in Fig. 10 were derived for atmospheric measurements,

15 and the surface area used to derive n_s was always based on measured particle number concentrations. Price et al. (2018) carried out airborne measurements in dust laden air over the tropical Atlantic. Parameterizations from McCluskey et al. (2018b)

were done for pristine SSA over the Northeast Atlantic and both laboratory and atmospheric measurements of SSA were the base for the n_s parameterization given in DeMott et al. (2016). n_s derived for our study coincides with the upper range of parameterizations that are otherwise reported for SSA but are clearly lower than values reported for atmospheric desert dust aerosol. This is striking since, as discussed above, INPs observed in this study most likely do not originate from sea spray.

5   This raises the question if and how n_s should be used to parameterize atmospheric INP measurements, which, however, is a question far too prominent to be answered in this study.

5   Summary and conclusions

The MarParCloud campaign took place in September and October 2018 on the island of Cape Verde to investigate aerosols prevailing in the Atlantic Ocean. In addition to a thorough analysis of the atmospheric aerosol particles and CCN in a compan-

10   ion paper (Gong et al., 2019b), samples collected for INPs analysis in this study include: sea surface microlayer (SML) and underlying water (ULW) from the ocean upwind of the island; quartz fiber filter samples of atmospheric aerosol, collected on a tower installed at the island shore and on a 744 m high mountaintop, as well as cloud water collected during cloud events on the mountaintop. N_INP were measured offline with two types of freezing devices, yielding results in the temperature range from roughly -5 to $-25\,°C$.

15   Both enrichment and depletion of N_INP in SML to ULW were observed. The enrichment factors (EF) varied from 0.36 to 11.40 and from 0.36 to 7.11 at -15 and $-20\,°C$, respectively, and were generally independent of the freezing temperature.

The measured N_INP in this study is consistent with the previous study of Welti et al. (2018), who characterized INPs sampled at CVAO over a time period of 4 years. A few CVAO PM_{10} filter samples (CVAO 1596, CVAO 1641 and CVAO 1643) showed elevated N_INP at high temperatures, e.g., above 0.01 std L^{-1} at $-10°C$. Biological particles usually contributed the INPs at this

20   moderate supercooling temperatures (Kanji et al., 2017; O'Sullivan et al., 2018).

About $83\pm22\%$, $67\pm18\%$ and $77\pm14\%$ (median$\pm$standard deviation) of INPs had a diameter $>1\,\mu m$ at ice activation temperatures of -12, -15, and $-18\,°C$, respectively, and over the whole examined temperature range, on average roughly 70% of all INPs were super-micron, independent of the temperature. The highly ice active INPs were not found on the CVAO PM_1 filters, which suggests that most of these likely biological INPs are in the super-micron size range.

25   N_INP were quite similar at CVAO and MV during non-cloud events. During cloud events, most INPs at MV were activated into cloud droplets. These findings aligned very well with the companion paper, i.e., during non-cloud events, PNSDs and N_CCN are similar at CVAO and MV, while during cloud events, larger particles at MV are activated to clouds. When highly ice active particles were present on CVAO PM_{10} filters, they were not observed on MV PM_{10} filters, but were instead observed in the respective cloud water samples. This shows that these INPs are activated into cloud droplets during cloud events.

30   By comparing N_INP derived for the different examined samples, it was found that values in air and in cloud water agreed well. We also compared atmospheric N_INP to those in SML and ULW, based on the ratio of sodium chloride concentrations measured for the atmosphere and for SML and ULW. From that we concluded that marine INPs from sea spray can only explain a small fraction of all atmospheric INPs at Cape Verde, unless there would be an enrichment of INPs from SML to the

atmosphere by at least a factor of 10^4. Such an enrichment, however, is higher than anything observed for organic compounds in super-micron particles so far. Generally low INP concentrations are found over remote oceanic regions, compared to locations closer to land masses, implying that the ocean is a weak source of INPs, compared to land. Summarizing, it can be assumed that most atmospheric INPs detected in the present study were mainly contributed by the dust particles at cold temperatures

5 possibly with few contributions from biological particles at warmer temperatures.

Data availability. The data are available through the World Data Center PANGAEA (https://www.pangaea.de/) in the near future. A link to the data can be found under this paper's assets tab on ACP's journal website.

Author contributions. X. Gong wrote the manuscript with contributions from H. Wex and M. van Pinxteren. C. Stolle, N. Triesch and B. Robinson collected ocean water samples. X. Gong, M. van Pinxteren and N. Triesch collected filter samples. K. W. Fomba collected cloud

10 water samples. X. Gong and J. Lubitz performed INP measurements. X. Gong preformed data evaluation. X. Gong, H. Wex and F. Stratmann discussed the results and further analysis after the campaign. All co-authors proofread and commented the manuscript.

Competing interests. The authors declare that they have no conflict of interests.

Acknowledgements. The works were carried out in the framework of the MarParCloud project. The authors acknowledge the Leibniz Association SAW funding for the project "Marine biological production, organic aerosol particles and marine clouds: a Process Chain (MarParCloud)", SAW-2016-TROPOS-2.

References

Agresti, A. and Coull, B. A.: Approximate is Better than ''Exact" for Interval Estimation of Binomial Proportions, The American Statistician, 52, 119–126, https://doi.org/10.1080/00031305.1998.10480550, https://doi.org/10.1080/00031305.1998.10480550, 1998.

Ansmann, A., Tesche, M., Althausen, D., Müller, D., Seifert, P., Freudenthaler, V., Heese, B., Wiegner, M., Pisani, G., Knippertz, P., and Dubovik, O.: Influence of Saharan dust on cloud glaciation in southern Morocco during the Saharan Mineral Dust Experiment, Journal of Geophysical Research: Atmospheres, 113, https://doi.org/10.1029/2007jd008785, https://agupubs.onlinelibrary.wiley.com/doi/abs/10.1029/2007JD008785, 2008.

Atkinson, J. D., Murray, B. J., Woodhouse, M. T., Whale, T. F., Baustian, K. J., Carslaw, K. S., Dobbie, S., O'Sullivan, D., and Malkin, T. L.: The importance of feldspar for ice nucleation by mineral dust in mixed-phase clouds, Nature, 498, 355, https://doi.org/10.1038/nature12278 https://www.nature.com/articles/nature12278#supplementary-information, https://doi.org/10.1038/nature12278, 2013.

Augustin-Bauditz, S., Wex, H., Kanter, S., Ebert, M., Niedermeier, D., Stolz, F., Prager, A., and Stratmann, F.: The immersion mode ice nucleation behavior of mineral dusts: A comparison of different pure and surface modified dusts, Geophysical Research Letters, 41, 7375–7382, https://doi.org/10.1002/2014gl061317, https://agupubs.onlinelibrary.wiley.com/doi/abs/10.1002/2014GL061317, 2014.

Bigg, E. K.: Ice Nucleus Concentrations in Remote Areas, Journal of the Atmospheric Sciences, 30, 1153–1157, https://doi.org/doi:10.1175/1520-0469(1973)030<1153:INCIRA>2.0.CO;2, http://journals.ametsoc.org/doi/abs/10.1175/1520-0469%281973%29030%3C1153%3AINCIRA%3E2.0.CO%3B2, 1973.

Boose, Y., Welti, A., Atkinson, J., Ramelli, F., Danielczok, A., Bingemer, H. G., Plötze, M., Sierau, B., Kanji, Z. A., and Lohmann, U.: Heterogeneous ice nucleation on dust particles sourced from nine deserts worldwide – Part 1: Immersion freezing, Atmospheric Chemistry and Physics, 16, 15075–15095, https://doi.org/10.5194/acp-16-15075-2016, https://www.atmos-chem-phys.net/16/15075/2016/, 2016.

Bréon, F.-M., Tanré, D., and Generoso, S.: Aerosol Effect on Cloud Droplet Size Monitored from Satellite, Science, 295, 834–838, https://doi.org/10.1126/science.1066434, https://science.sciencemag.org/content/sci/295/5556/834.full.pdf, 2002.

Brier, G. W. and Kline, D. B.: Ocean Water as a Source of Ice Nuclei, Science, 130, 717–718, https://doi.org/10.1126/science.130.3377.717, 1959.

Budke, C. and Koop, T.: BINARY: an optical freezing array for assessing temperature and time dependence of heterogeneous ice nucleation, Atmos. Meas. Tech., 8, 689–703, https://doi.org/10.5194/amt-8-689-2015, http://www.atmos-meas-tech.net/8/689/2015/, 2015.

Burrows, S. M., Hoose, C., Pöschl, U., and Lawrence, M. G.: Ice nuclei in marine air: biogenic particles or dust?, Atmos. Chem. Phys., 13, 245–267, https://doi.org/10.5194/acp-13-245-2013, https://www.atmos-chem-phys.net/13/245/2013/, 2013.

Chen, J., Wu, Z., Augustin-Bauditz, S., Grawe, S., Hartmann, M., Pei, X., Liu, Z., Ji, D., and Wex, H.: Ice-nucleating particle concentrations unaffected by urban air pollution in Beijing, China, Atmos. Chem. Phys., 18, 3523–3539, https://doi.org/10.5194/acp-18-3523-2018, https://www.atmos-chem-phys.net/18/3523/2018/, 2018.

Chou, C., Stetzer, O., Weingartner, E., Jurányi, Z., Kanji, Z. A., and Lohmann, U.: Ice nuclei properties within a Saharan dust event at the Jungfraujoch in the Swiss Alps, Atmos. Chem. Phys., 11, 4725–4738, https://doi.org/10.5194/acp-11-4725-2011, http://www.atmos-chem-phys.net/11/4725/2011/, 2011.

Conen, F., Henne, S., Morris, C. E., and Alewell, C.: Atmospheric ice nucleators active $\geq$-12°C can be quantified on PM_{10} filters, Atmos. Meas. Tech., 5, 321–327, https://doi.org/10.5194/amt-5-321-2012, https://www.atmos-meas-tech.net/5/321/2012/, 2012.

Conen, F., Eckhardt, S., Gundersen, H., Stohl, A., and Yttri, K. E.: Rainfall drives atmospheric ice-nucleating particles in the coastal climate of southern Norway, Atmos. Chem. Phys., 17, 11 065–11 073, https://doi.org/10.5194/acp-17-11065-2017, https://www.atmos-chem-phys. net/17/11065/2017/, 2017.

Creamean, J. M., Kirpes, R. M., Pratt, K. A., Spada, N. J., Maahn, M., de Boer, G., Schnell, R. C., and China, S.: Marine and terrestrial

5   influences on ice nucleating particles during continuous springtime measurements in an Arctic oilfield location, Atmos. Chem. Phys., 18, 18 023–18 042, https://doi.org/10.5194/acp-18-18023-2018, https://www.atmos-chem-phys.net/18/18023/2018/, 2018.

DeMott, P. J., Sassen, K., Poellot, M. R., Baumgardner, D., Rogers, D. C., Brooks, S. D., Prenni, A. J., and Kreidenweis, S. M.: African dust aerosols as atmospheric ice nuclei, Geophysical Research Letters, 30, n/a–n/a, https://doi.org/10.1029/2003GL017410, http://dx.doi.org/ 10.1029/2003GL017410, 2003.

10   DeMott, P. J., Prenni, A. J., Liu, X., Kreidenweis, S. M., Petters, M. D., Twohy, C. H., Richardson, M. S., Eidhammer, T., and Rogers, D. C.: Predicting global atmospheric ice nuclei distributions and their impacts on climate, Proceedings of the National Academy of Sciences, 107, 11 217–11 222, https://doi.org/10.1073/pnas.0910818107, http://www.pnas.org/content/107/25/11217.abstract, 2010.

DeMott, P. J., Prenni, A. J., McMeeking, G. R., Sullivan, R. C., Petters, M. D., Tobo, Y., Niemand, M., Möhler, O., Snider, J. R., Wang, Z., and Kreidenweis, S. M.: Integrating laboratory and field data to quantify the immersion freezing ice nucleation activity of mineral dust

15   particles, Atmos. Chem. Phys., 15, 393–409, https://doi.org/10.5194/acp-15-393-2015, https://www.atmos-chem-phys.net/15/393/2015/, 2015.

DeMott, P. J., Hill, T. C. J., McCluskey, C. S., Prather, K. A., Collins, D. B., Sullivan, R. C., Ruppel, M. J., Mason, R. H., Irish, V. E., Lee, T., Hwang, C. Y., Rhee, T. S., Snider, J. R., McMeeking, G. R., Dhaniyala, S., Lewis, E. R., Wentzell, J. J. B., Abbatt, J., Lee, C., Sultana, C. M., Ault, A. P., Axson, J. L., Diaz Martinez, M., Venero, I., Santos-Figueroa, G., Stokes, M. D., Deane, G. B., Mayol-

20   Bracero, O. L., Grassian, V. H., Bertram, T. H., Bertram, A. K., Moffett, B. F., and Franc, G. D.: Sea spray aerosol as a unique source of ice nucleating particles, Proceedings of the National Academy of Sciences, 113, 5797–5803, https://doi.org/10.1073/pnas.1514034112, http://www.pnas.org/content/113/21/5797.abstract, 2016.

Demoz, B. B., Collett, J. L., and Daube, B. C.: On the Caltech Active Strand Cloudwater Collectors, Atmospheric Research, 41, 47–62, https://doi.org/https://doi.org/10.1016/0169-8095(95)00044-5, http://www.sciencedirect.com/science/article/pii/0169809595000445,

25   1996.

Gioda, A., Mayol-Bracero, O. L., Morales-García, F., Collett, J., Decesari, S., Emblico, L., Facchini, M. C., Morales-De Jesús, R. J., Mertes, S., Borrmann, S., Walter, S., and Schneider, J.: Chemical Composition of Cloud Water in the Puerto Rican Tropical Trade Wind Cumuli, Water, Air, and Soil Pollution, 200, 3–14, https://doi.org/10.1007/s11270-008-9888-4, https://doi.org/10.1007/s11270-008-9888-4, 2009.

Gong, X., Wex, H., Müller, T., Wiedensohler, A., Höhler, K., Kandler, K., Ma, N., Dietel, B., Schiebel, T., Möhler, O., and Stratmann, F.:

30   Characterization of aerosol properties at Cyprus, focusing on cloud condensation nuclei and ice nucleating particles, Atmos. Chem. Phys. Discuss., 2019, 1–34, https://doi.org/10.5194/acp-2019-198, https://www.atmos-chem-phys-discuss.net/acp-2019-198/, 2019a.

Gong, X., Wex, H., Voigtländer, J., Fomba, K. W., Weinhold, K., van Pinxteren, M., Henning, S., Müller, T., Herrmann, H., and Stratmann, F.: Characterization of aerosol particles at Cape Verde close to sea and cloud level heights – Part 1: particle number size distribution, cloud condensation nuclei and their origins, Atmos. Chem. Phys. Discuss., 2019, 1–31, https://doi.org/10.5194/acp-2019-585, https://

35   www.atmos-chem-phys-discuss.net/acp-2019-585/, 2019b.

Hartmann, M., Blunier, T., Brügger, S., Schmale, J., Schwikowski, M., Vogel, A., Wex, H., and Stratmann, F.: Variation of Ice Nucleating Particles in the European Arctic Over the Last Centuries, Geophysical Research Letters, 0, https://doi.org/10.1029/2019gl082311, https: //agupubs.onlinelibrary.wiley.com/doi/abs/10.1029/2019GL082311, 2019.

Harvey, G. W. and Burzell, L. A.: A simple microlayer method for small samples, Limnology and Oceanography, 17, 156–157, https://doi.org/doi:10.4319/lo.1972.17.1.0156, https://aslopubs.onlinelibrary.wiley.com/doi/abs/10.4319/lo.1972.17.1.0156, 1972.

Hoose, C. and Möhler, O.: Heterogeneous ice nucleation on atmospheric aerosols: a review of results from laboratory experiments, Atmos. Chem. Phys., 12, 9817–9854, https://doi.org/10.5194/acp-12-9817-2012, http://www.atmos-chem-phys.net/12/9817/2012/, 2012.

5 Huffman, J. A., Prenni, A. J., DeMott, P. J., Pöhlker, C., Mason, R. H., Robinson, N. H., Fröhlich-Nowoisky, J., Tobo, Y., Després, V. R., Garcia, E., Gochis, D. J., Harris, E., Müller-Germann, I., Ruzene, C., Schmer, B., Sinha, B., Day, D. A., Andreae, M. O., Jimenez, J. L., Gallagher, M., Kreidenweis, S. M., Bertram, A. K., and Pöschl, U.: High concentrations of biological aerosol particles and ice nuclei during and after rain, Atmos. Chem. Phys., 13, 6151–6164, https://doi.org/10.5194/acp-13-6151-2013, https://www.atmos-chem-phys.net/13/6151/2013/, 2013.

10 Igel, A. L. and Heever, S. C. v. d.: The Importance of the Shape of Cloud Droplet Size Distributions in Shallow Cumulus Clouds. Part II: Bulk Microphysics Simulations, Journal of the Atmospheric Sciences, 74, 259–273, https://doi.org/10.1175/jas-d-15-0383.1, https://journals.ametsoc.org/doi/abs/10.1175/JAS-D-15-0383.1, 2017.

Irish, V. E., Elizondo, P., Chen, J., Chou, C., Charette, J., Lizotte, M., Ladino, L. A., Wilson, T. W., Gosselin, M., Murray, B. J., Polishchuk, E., Abbatt, J. P. D., Miller, L. A., and Bertram, A. K.: Ice-nucleating particles in Canadian Arctic sea-surface microlayer and bulk seawater, 15 Atmos. Chem. Phys., 17, 10 583–10 595, https://doi.org/10.5194/acp-17-10583-2017, https://www.atmos-chem-phys.net/17/10583/2017/, 2017.

Irish, V. E., Hanna, S. J., Willis, M. D., China, S., Thomas, J. L., Wentzell, J. J. B., Cirisan, A., Si, M., Leaitch, W. R., Murphy, J. G., Abbatt, J. P. D., Laskin, A., Girard, E., and Bertram, A. K.: Ice nucleating particles in the marine boundary layer in the Canadian Arctic during summer 2014, Atmos. Chem. Phys., 19, 1027–1039, https://doi.org/10.5194/acp-19-1027-2019, https://www.atmos-chem-phys. 20 net/19/1027/2019/, 2019a.

Irish, V. E., Hanna, S. J., Xi, Y., Boyer, M., Polishchuk, E., Ahmed, M., Chen, J., Abbatt, J. P. D., Gosselin, M., Chang, R., Miller, L. A., and Bertram, A. K.: Revisiting properties and concentrations of ice-nucleating particles in the sea surface microlayer and bulk seawater in the Canadian Arctic during summer, Atmos. Chem. Phys., 19, 7775–7787, https://doi.org/10.5194/acp-19-7775-2019, https://www. atmos-chem-phys.net/19/7775/2019/, 2019b.

25 Joly, M., Amato, P., Deguillaume, L., Monier, M., Hoose, C., and Delort, A. M.: Quantification of ice nuclei active at near 0 °C temperatures in low-altitude clouds at the Puy de Dôme atmospheric station, Atmos. Chem. Phys., 14, 8185–8195, https://doi.org/10.5194/acp-14-8185-2014, https://www.atmos-chem-phys.net/14/8185/2014/, 2014.

Kanji, Z. A., Ladino, L. A., Wex, H., Boose, Y., Burkert-Kohn, M., Cziczo, D. J., and Krämer, M.: Overview of Ice Nucleating Particles, Meteorological Monographs, 58, 1.1–1.33, https://doi.org/10.1175/amsmonographs-d-16-0006.1, https://journals.ametsoc.org/doi/abs/10. 30 1175/AMSMONOGRAPHS-D-16-0006.1, 2017.

Keene, W. C., Maring, H., Maben, J. R., Kieber, D. J., Pszenny, A. A. P., Dahl, E. E., Izaguirre, M. A., Davis, A. J., Long, M. S., Zhou, X., Smoydzin, L., and Sander, R.: Chemical and physical characteristics of nascent aerosols produced by bursting bubbles at a model air-sea interface, Journal of Geophysical Research: Atmospheres, 112, https://doi.org/10.1029/2007jd008464, https://agupubs.onlinelibrary. wiley.com/doi/abs/10.1029/2007JD008464, 2007.

35 Koop, T. and Zobrist, B.: Parameterizations for ice nucleation in biological and atmospheric systems, Physical Chemistry Chemical Physics, 11, 10 839–10 850, https://doi.org/10.1039/B914289D, http://dx.doi.org/10.1039/B914289D, 2009.

Kreidenweis, S., Koehler, K., DeMott, P., Prenni, A., Carrico, C., and Ervens, B.: Water activity and activation diameters from hygroscopicity data-Part I: Theory and application to inorganic salts, Atmospheric Chemistry and Physics, 5, 1357–1370, 2005.

Mason, R. H., Si, M., Chou, C., Irish, V. E., Dickie, R., Elizondo, P., Wong, R., Brintnell, M., Elsasser, M., Lassar, W. M., Pierce, K. M., Leaitch, W. R., MacDonald, A. M., Platt, A., Toom-Sauntry, D., Sarda-Estève, R., Schiller, C. L., Suski, K. J., Hill, T. C. J., Abbatt, J. P. D., Huffman, J. A., DeMott, P. J., and Bertram, A. K.: Size-resolved measurements of ice-nucleating particles at six locations in North America and one in Europe, Atmos. Chem. Phys., 16, 1637–1651, https://doi.org/10.5194/acp-16-1637-2016, https://www.atmos-chem-phys.net/16/1637/2016/, 2016.

McCluskey, C. S., Hill, T. C. J., Humphries, R. S., Rauker, A. M., Moreau, S., Strutton, P. G., Chambers, S. D., Williams, A. G., McRobert, I., Ward, J., Keywood, M. D., Harnwell, J., Ponsonby, W., Loh, Z. M., Krummel, P. B., Protat, A., Kreidenweis, S. M., and DeMott, P. J.: Observations of Ice Nucleating Particles Over Southern Ocean Waters, Geophysical Research Letters, 45, 11,989–11,997, https://doi.org/10.1029/2018GL079981, https://doi.org/10.1029/2018GL079981, 2018a.

McCluskey, C. S., Ovadnevaite, J., Rinaldi, M., Atkinson, J., Belosi, F., Ceburnis, D., Marullo, S., Hill, T. C. J., Lohmann, U., Kanji, Z. A., O'Dowd, C., Kreidenweis, S. M., and DeMott, P. J.: Marine and Terrestrial Organic Ice-Nucleating Particles in Pristine Marine to Continentally Influenced Northeast Atlantic Air Masses, Journal of Geophysical Research: Atmospheres, 123, 6196–6212, https://doi.org/doi:10.1029/2017JD028033, https://agupubs.onlinelibrary.wiley.com/doi/abs/10.1029/2017JD028033, 2018b.

Mertes, S., Verheggen, B., Walter, S., Connolly, P., Ebert, M., Schneider, J., Bower, K. N., Cozic, J., Weinbruch, S., Baltensperger, U., and Weingartner, E.: Counterflow Virtual Impactor Based Collection of Small Ice Particles in Mixed-Phase Clouds for the Physico-Chemical Characterization of Tropospheric Ice Nuclei: Sampler Description and First Case Study, Aerosol Science and Technology, 41, 848–864, https://doi.org/10.1080/02786820701501881, https://doi.org/10.1080/02786820701501881, 2007.

Miles, N. L., Verlinde, J., and Clothiaux, E. E.: Cloud Droplet Size Distributions in Low-Level Stratiform Clouds, Journal of the Atmospheric Sciences, 57, 295–311, https://doi.org/10.1175/1520-0469(2000)057<0295:cdsdil>2.0.co;2, https://journals.ametsoc.org/doi/abs/10.1175/1520-0469%282000%29057%3C0295%3ACDSDIL%3E2.0.CO%3B2, 2000.

Murray, B. J., O'Sullivan, D., Atkinson, J. D., and Webb, M. E.: Ice nucleation by particles immersed in supercooled cloud droplets, Chemical Society Reviews, 41, 6519–6554, https://doi.org/10.1039/C2CS35200A, http://dx.doi.org/10.1039/C2CS35200A, 2012.

Niedermeier, D., Augustin-Bauditz, S., Hartmann, S., Wex, H., Ignatius, K., and Stratmann, F.: Can we define an asymptotic value for the ice active surface site density for heterogeneous ice nucleation?, Journal of Geophysical Research: Atmospheres, 120, 5036–5046, https://doi.org/10.1002/2014JD022814, https://agupubs.onlinelibrary.wiley.com/doi/abs/10.1002/2014JD022814, 2015.

Niemand, M., Möhler, O., Vogel, B., Vogel, H., Hoose, C., Connolly, P., Klein, H., Bingemer, H., DeMott, P., Skrotzki, J., and Leisner, T.: A Particle-Surface-Area-Based Parameterization of Immersion Freezing on Desert Dust Particles, Journal of the Atmospheric Sciences, 69, 3077–3092, https://doi.org/10.1175/jas-d-11-0249.1, http://journals.ametsoc.org/doi/abs/10.1175/JAS-D-11-0249.1, 2012.

O'Sullivan, D., Adams, M. P., Tarn, M. D., Harrison, A. D., Vergara-Temprado, J., Porter, G. C. E., Holden, M. A., Sanchez-Marroquin, A., Carotenuto, F., Whale, T. F., McQuaid, J. B., Walshaw, R., Hedges, D. H. P., Burke, I. T., Cui, Z., and Murray, B. J.: Contributions of biogenic material to the atmospheric ice-nucleating particle population in North Western Europe, Scientific Reports, 8, 13 821, https://doi.org/10.1038/s41598-018-31981-7, https://doi.org/10.1038/s41598-018-31981-7, 2018.

Petters, M. and Wright, T.: Revisiting ice nucleation from precipitation samples, Geophysical Research Letters, 42, 8758–8766, https://doi.org/doi:10.1002/2015GL065733, https://agupubs.onlinelibrary.wiley.com/doi/abs/10.1002/2015GL065733, 2015.

Price, H. C., Baustian, K. J., McQuaid, J. B., Blyth, A., Bower, K. N., Choularton, T., Cotton, R. J., Cui, Z., Field, P. R., Gallagher, M., Hawker, R., Merrington, A., Miltenberger, A., Neely III, R. R., Parker, S. T., Rosenberg, P. D., Taylor, J. W., Trembath, J., Vergara-Temprado, J., Whale, T. F., Wilson, T. W., Young, G., and Murray, B. J.: Atmospheric Ice-Nucleating Particles in the Dusty Tropical

Atlantic, Journal of Geophysical Research: Atmospheres, 123, 2175–2193, https://doi.org/doi:10.1002/2017JD027560, https://agupubs. onlinelibrary.wiley.com/doi/abs/10.1002/2017JD027560, 2018.

Pruppacher, H. and Klett, J.: Microphysics of Clouds and Precipitation, vol. 18, Springer Science & Business Media, 2010.

Pummer, B. G., Budke, C., Augustin-Bauditz, S., Niedermeier, D., Felgitsch, L., Kampf, C. J., Huber, R. G., Liedl, K. R., Loerting, T.,
5   Moschen, T., Schauperl, M., Tollinger, M., Morris, C. E., Wex, H., Grothe, H., Pöschl, U., Koop, T., and Fröhlich-Nowoisky, J.: Ice nucleation by water-soluble macromolecules, Atmos. Chem. Phys., 15, 4077–4091, https://doi.org/10.5194/acp-15-4077-2015, https:// www.atmos-chem-phys.net/15/4077/2015/, 2015.

Quinn, P. K., Collins, D. B., Grassian, V. H., Prather, K. A., and Bates, T. S.: Chemistry and Related Properties of Freshly Emitted Sea Spray Aerosol, Chemical Reviews, 115, 4383–4399, https://doi.org/10.1021/cr500713g, http://dx.doi.org/10.1021/cr500713g, 2015.

10 Rangno, A. L. and Hobbs, P. V.: Microstructures and precipitation development in cumulus and small cumulonimbus clouds over the warm pool of the tropical Pacific Ocean, Quarterly Journal of the Royal Meteorological Society, 131, 639–673, https://doi.org/10.1256/qj.04.13, https://rmets.onlinelibrary.wiley.com/doi/abs/10.1256/qj.04.13, 2005.

Robinson, T. B., Stolle, C., and Wurl, O.: Depth is Relative: The Importance of Depth on TEP in the Near Surface Environment, Ocean Sci. Discuss., 2019, 1–20, https://doi.org/10.5194/os-2019-79, https://www.ocean-sci-discuss.net/os-2019-79/, 2019.

15 Schnell, R. C.: Ice Nuclei in Seawater, Fog Water and Marine Air off the Coast of Nova Scotia: Summer 1975, Journal of the Atmospheric Sciences, 34, 1299–1305, https://doi.org/doi:10.1175/1520-0469(1977)034<1299:INISFW>2.0.CO;2, http://journals.ametsoc.org/ doi/abs/10.1175/1520-0469%281977%29034%3C1299%3AINISFW%3E2.0.CO%3B2, 1977.

Schnell, R. C. and Vali, G.: Biogenic Ice Nuclei: Part I. Terrestrial and Marine Sources, Journal of the Atmospheric Sciences, 33, 1554–1564, https://doi.org/doi:10.1175/1520-0469(1976)033<1554:BINPIT>2.0.CO;2, http://journals.ametsoc.org/doi/abs/10.1175/
20   1520-0469%281976%29033%3C1554%3ABINPIT%3E2.0.CO%3B2, 1976.

Schrod, J., Weber, D., Drücke, J., Keleshis, C., Pikridas, M., Ebert, M., Cvetković, B., Nickovic, S., Marinou, E., Baars, H., Ansmann, A., Vrekoussis, M., Mihalopoulos, N., Sciare, J., Curtius, J., and Bingemer, H. G.: Ice nucleating particles over the Eastern Mediterranean measured by unmanned aircraft systems, Atmos. Chem. Phys., 17, 4817–4835, https://doi.org/10.5194/acp-17-4817-2017, https://www. atmos-chem-phys.net/17/4817/2017/, 2017.

25 Si, M., Irish, V. E., Mason, R. H., Vergara-Temprado, J., Hanna, S. J., Ladino, L. A., Yakobi-Hancock, J. D., Schiller, C. L., Wentzell, J. J. B., Abbatt, J. P. D., Carslaw, K. S., Murray, B. J., and Bertram, A. K.: Ice-nucleating ability of aerosol particles and possible sources at three coastal marine sites, Atmos. Chem. Phys., 18, 15 669–15 685, https://doi.org/10.5194/acp-18-15669-2018, https://www.atmos-chem-phys. net/18/15669/2018/, 2018.

Suski, K. J., Hill, T. C. J., Levin, E. J. T., Miller, A., DeMott, P. J., and Kreidenweis, S. M.: Agricultural harvesting emissions of ice-
30   nucleating particles, Atmos. Chem. Phys., 18, 13 755–13 771, https://doi.org/10.5194/acp-18-13755-2018, https://www.atmos-chem-phys. net/18/13755/2018/, 2018.

Ullrich, R., Hoose, C., Möhler, O., Niemand, M., Wagner, R., Höhler, K., Hiranuma, N., Saathoff, H., and Leisner, T.: A New Ice Nucleation Active Site Parameterization for Desert Dust and Soot, Journal of the Atmospheric Sciences, 74, 699–717, https://doi.org/10.1175/JAS-D-16-0074.1, https://doi.org/10.1175/JAS-D-16-0074.1, 2017.

35 Vali, G.: Sizes of Atmospheric Ice Nuclei, Nature, 212, 384–385, https://doi.org/10.1038/212384a0, https://doi.org/10.1038/212384a0, 1966.

Vali, G.: Quantitative Evaluation of Experimental Results an the Heterogeneous Freezing Nucleation of Supercooled Liquids, Journal of the Atmospheric Sciences, 28, 402–409, https://doi.org/10.1175/1520-0469(1971)028<0402:qeoera>2.0.co;2, http://journals.ametsoc.org/ doi/abs/10.1175/1520-0469%281971%29028%3C0402%3AQEOERA%3E2.0.CO%3B2, 1971.

Vali, G., DeMott, P. J., Möhler, O., and Whale, T. F.: Technical Note: A proposal for ice nucleation terminology, Atmos. Chem. Phys., 15, 10 263–10 270, https://doi.org/10.5194/acp-15-10263-2015, https://www.atmos-chem-phys.net/15/10263/2015/, 2015.

van Pinxteren, M., Barthel, S., Fomba, K. W., Müller, K., Von Tümpling, W., and Herrmann, H.: The influence of environmental drivers on the enrichment of organic carbon in the sea surface microlayer and in submicron aerosol particles–measurements from the Atlantic Ocean, Elementa: Science of the Anthropocene, 5, 35, 2017.

Welti, A., Müller, K., Fleming, Z. L., and Stratmann, F.: Concentration and variability of ice nuclei in the subtropical maritime boundary layer, Atmospheric Chemistry and Physics, 18, 5307–5320, 2018.

Westbrook, C. D. and Illingworth, A. J.: The formation of ice in a long-lived supercooled layer cloud, Quarterly Journal of the Royal Meteorological Society, 139, 2209–2221, https://doi.org/10.1002/qj.2096, https://rmets.onlinelibrary.wiley.com/doi/abs/10.1002/qj.2096, 2013.

Wex, H., Huang, L., Zhang, W., Hung, H., Traversi, R., Becagli, S., Sheesley, R. J., Moffett, C. E., Barrett, T. E., Bossi, R., Skov, H., Hünerbein, A., Lubitz, J., Löffler, M., Linke, O., Hartmann, M., Herenz, P., and Stratmann, F.: Annual variability of ice-nucleating particle concentrations at different Arctic locations, Atmos. Chem. Phys., 19, 5293–5311, https://doi.org/10.5194/acp-19-5293-2019, https://www.atmos-chem-phys.net/19/5293/2019/, 2019.

Wilson, T. W., Ladino, L. A., Alpert, P. A., Breckels, M. N., Brooks, I. M., Browse, J., Burrows, S. M., Carslaw, K. S., Huffman, J. A., Judd, C., Kilthau, W. P., Mason, R. H., McFiggans, G., Miller, L. A., Najera, J. J., Polishchuk, E., Rae, S., Schiller, C. L., Si, M., Temprado, J. V., Whale, T. F., Wong, J. P. S., Wurl, O., Yakobi-Hancock, J. D., Abbatt, J. P. D., Aller, J. Y., Bertram, A. K., Knopf, D. A., and Murray, B. J.: A marine biogenic source of atmospheric ice-nucleating particles, Nature, 525, 234–238, https://doi.org/10.1038/nature14986, http://dx.doi.org/10.1038/nature14986, 2015.